Published in final edited form as:

Immunity. 2019 March 19; 50(3): 591–599.e6. doi:10.1016/j.immuni.2019.02.009.

Viral DNA Binding to NLRC3, an Inhibitory Nucleic Acid Sensor, Unleashes STING, a Cyclic Dinucleotide Receptor that Activates Type I Interferon

Xin Li[#1], **Meng Deng**[#1,3], **Alex S. Petrucelli**[1], **Cheng Zhu**[4], **Jinyao Mo**[5], **Lu Zhang**[1,6], **Jason W. Tam**[1], **Pablo Ariel**[7], **Baoyu Zhao**[8], **Song Zhang**[1], **Hengming Ke**[4], **Pingwei Li**[8], **Nikolay V. Dokholyan**[1,4,9], **Joseph A. Duncan**[5], and **Jenny P.-Y. Ting**[1,2,11,*]

[1]Lineberger Comprehensive Cancer Center, University of North Carolina at Chapel Hill, Chapel Hill, NC 27599, USA

[2]Department of Genetics, University of North Carolina at Chapel Hill, Chapel Hill, NC 27599, USA

[3]Oral and Craniofacial Biomedicine PhD Program, School of Dentistry, University of North Carolina at Chapel Hill, Chapel Hill, NC 27599, USA

[4]Department of Biochemistry and Biophysics, University of North Carolina, Chapel Hill, NC 27599, USA

[5]Department of Medicine, Division of Infectious Diseases, University of North Carolina, Chapel Hill, NC 27599, USA

[6]Sarah W. Stedman Nutrition and Metabolism Center and Duke Molecular Physiology Institute, Duke University Medical Center, Durham, NC 27701, USA

[7]Department of Pathology and Laboratory Medicine, University of North Carolina, Chapel Hill, NC 27599, USA

[8]Department of Biochemistry and Biophysics, Texas A&M University, College Station, TX 77843, USA

[9]Departments of Pharmacology and Biochemistry and Molecular Biology, Penn State College of Medicine, PA 17033, USA

[11]Lead Contact

[#] These authors contributed equally to this work.

[*]Correspondence: jenny_ting@med.unc.edu.

AUTHOR CONTRIBUTIONS

X.L., M.D., A.S.P., and J.P.-Y.T. designed the experiments; X.L. and J.P.-Y.T. wrote the manuscript with critical input from A.S.P., H.M.K., and J.A.D; X.L. performed all of the protein and biochemistry experiments; M.D. contributed all of the cellular assays; A.S.P. performed confocal microcopy assays; A.S.P. and P.A. performed analysis of microscopy data; C.Z. and N.V.D. performed the structural modeling and MD simulations; J.Y.M. and J.A.D. generated the baculoviral recombinant NLRC3 and NLRX1 proteins; L.Z. and J.W.T. contributed to experiments involving MEFs; B.Y.Z. and P.W.L. contributed to STING *E. coli* expression plasmid and modified pET-28a-SUMO vector; and S.Z. generated BMDMs. All contributing authors agreed to the submission of this manuscript for publication.

SUPPLEMENTAL INFORMATION

Supplemental Information can be found with the article online at https://doi.org/10.1016/j.immuni.2019.02.009.

DECLARATION OF INTERESTS

The authors declare no competing financial interests.

SUMMARY

Immune suppression is a crucial component of immunoregulation and a subgroup of nucleotidebinding domain (NBD), leucine-rich repeat (LRR)-containing proteins (NLRs) attenuate innate immunity. How this inhibitory function is controlled is unknown. A key question is whether microbial ligands can regulate this inhibition. NLRC3 is a negative regulator that attenuates type I interferon (IFN-I) response by sequestering and attenuating stimulator of interferon genes (STING) activation. Here, we report that NLRC3 binds viral DNA and other nucleic acids through its LRR domain. DNA binding to NLRC3 increases its ATPase activity, and ATP-binding by NLRC3 diminishes its interaction with STING, thus licensing an IFN-I response. This work uncovers a mechanism wherein viral nucleic acid binding releases an inhibitory innate receptor from its target.

Graphical Abstract

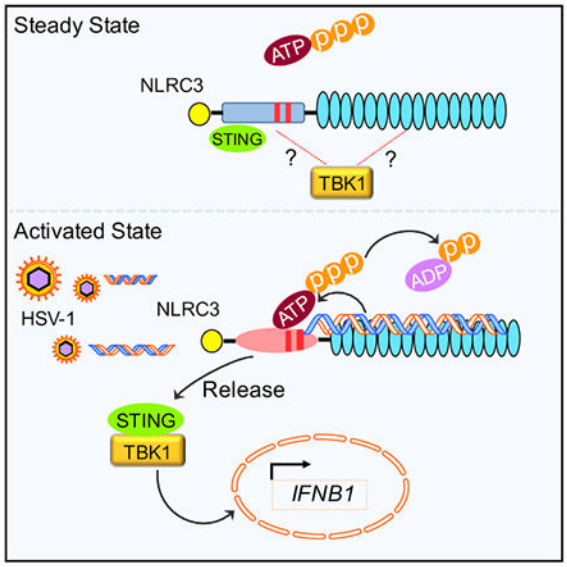

In Brief

NLRC3 is a negative regulator that attenuates type I interferon by sequestering STING and TBK1 activation, but the ligand of NLRC3 is unknown. Li et al. demonstrate that viral DNA directly binds to NLRC3 through the LRR domain, which enhances its ATPase activity and unleashes its interaction with STING and TBK1.

INTRODUCTION

Members of the nucleotide-binding domain (NBD) and leucinerich repeat (LRR)-containing family (also known as NOD-like receptors [NLRs]) can respond to pathogen-associated molecular patterns (PAMPs) from microbial pathogens and damage-associated molecular patterns (DAMPs) from the host (Guo et al., 2015). There are at least 22 NLR proteins in this large family of innate immune receptors (Harton et al., 2002). The most studied NLRs, including NLRP3, NLRC4, and NLRP6, trigger inflammasome activation leading to

caspase-1 activation (Elinav et al., 2011; Guo et al., 2015). However, the ligands for these are sporadically known. NLRC4 indirectly interacts with the needle and rod of the bacterial type 3 secretion system and flagellin through various neuronal apoptosis inhibitory proteins (NAIPs) (Kofoed and Vance, 2011; Zhao et al., 2011). Additionally, NOD1 and NOD2 interact with bacterial peptidoglycans (Chamaillard et al., 2003; Girardin et al., 2003a; Girardin et al., 2003b; Mo et al., 2012). Recently, lipoteichoic acid (LTA), which is from Gram-positive bacteria, has been reported to be a ligand for NLRP6 and to trigger NLRP6 inflammasomes (Hara et al., 2018). Ligands for other NLRs remain a major missing link in the field, and no viral PAMPs for NLR have been clearly identified.

Equally important, a subgroup of NLRs attenuate rather than activate immune signaling, yet their putative ligands, if any, are completely unknown. One such regulator is NLRC3 (CLR16.2) (Conti et al., 2005; Harton et al., 2002), which reduces NF-κb activation (Schneider et al., 2012b), diminishes stimulator of interferon genes (STING) and TANK-binding kinase 1 (TBK1) activation of type I interferon (IFN-I) during infection (Zhang et al., 2014), and decreases the mammalian target of rapamycin (mTOR) nutrient sensor signaling in colon cancer (Karki et al., 2016). Recently, we and others discovered that *Nlrc3* restricts autoimmune and virus-specific $CD4^+$ T cell responses by attenuating T cell signaling (Hu et al., 2018; Uchimura et al., 2018).

The concept of immune suppression is a recent but central premise in immunology, especially in the context of adaptive immunity, where modulation can prevent autoimmunity or enhance cancer immunotherapy. However, the field of immune suppression in innate immunity is nascent, and little mechanistic understanding of how negative regulation of innate immunity is achieved. A central insight that is needed to understand the mechanism of NLR-mediated innate immune suppression is the ligands for inhibitory NLRs, such as NLRC3.

In this study, we used multiple biochemical methods employing both cell-based assays and cell-free recombinant proteins to show that double-stranded DNA (dsDNA) from herpes simplex virus 1 (HSV-1) directly binds NLRC3 with high affinity. Structural modeling followed by functional verification has identified the first four LRRs of NLRC3 as important for DNA binding to NLRC3. Furthermore, dsDNA binding to the LRR of NLRC3 allosterically enhances ATPase activity of the adjacent NBD by 10-fold, and this change is associated with the separation of STING from the NBD domain. Collectively, our work unveils a pathway wherein viral DNA binding causes NLRC3 to release itself from STING and thus liberates STING to activate the interferon pathway.

RESULTS

NLRC3 Directly Interacts with Herpes Simplex Virus dsDNA

To show the known inhibitory function of NLRC3 to DNA-induced IFN-I production (Zhang et al., 2014), we generated mouse embryonic fibroblasts (MEFs) from wild-type (WT) and *Nlrc3*$^{-/-}$ mice. *Nlrc3*$^{-/-}$ MEFs had enhanced *Ifnb* expression in response to HSV-1 infection, which provided a physiologic context (Figure 1A). Several DNA-binding innate immune receptors, including cGAS (Sun et al., 2013), AIM2 (Bürckstümmer et al.,

2009; Fernandes-Alnemri et al., 2009; Hornung et al., 2009), IFI16 (Unterholzner et al., 2010), and DDX41 (Zhang et al., 2011), have been reported in the literature. In all cases, DNA recognition activates innate immunity. In contrast, DNA binding has not been shown to regulate an inhibitory innate immune receptor. To explore whether NLRC3 could bind DNA, we transfected biotinylated-HSV-60 dsDNA and showed that it efficiently precipitated hemagglutinin (HA)-tagged human NLRC3 and the positive controls IFI16, DDX41, and cGAS but not another NLR, NLRX1, STING, or the RNA-binding protein RIG-I from 293T lysates (Figures 1B and S1A). In addition, when overexpressed NLRC3 was silenced by short hairpin RNA (shRNA) in HEK293T cells, as shown by a reduction of the transcript (Figure S1B), NLRC3-DNA binding was abrogated by this silencing (Figure S1C). The caspase activation and recruitment domain (CARD) of human caspases 4 and 5 and mouse caspase 11 recognized cytosolic (lipopolysaccharide) LPS (Shi et al., 2014). NLRC3 also contains a CARD, but it was not precipitated by biotinylated LPS, which served as a specificity control (Figure S1D). Furthermore, we show that free HSV60 dsDNA, but not free LPS, could compete with biotin-HSV60 dsDNA binding to NLRC3, thus showing that the binding is specific. (Figure 1C). Additionally, we co-transfected HA-NLRC3 or a control HA-NLRX1 with HSV-60 dsDNA in HEK293T cells, used formaldehyde to crosslink cellular proteins and nucleic acids, and then performed anti-HA pull-down. HSV-60 DNA associated with NLRC3 but not NLRX1, as determined by the amplification of bound DNA with HSV-60-specific primers (Figure 1D).

To more definitively determine whether NLRC3 directly binds DNA, we expressed and purified NLRC3^{FL} (full-length) protein in insect cells (Figure S2A). Purified cGAS^{FL} protein from *E.coli* and NLRX1^{FL} protein from insect cells were also produced as controls. (Figures S2B and S2C). Biotinylated 60 bp (Bio-HSV-60) and 15 bp HSV-60 (Bio-HSV-15) dsDNA robustly bound recombinant NLRC3^{FL} protein, but not NLRX1^{FL} protein (Figure 1E). In an electrophoretic mobility shift assay (EMSA) where HSV-60 dsDNA was incubated with recombinant NLRC3^{FL}, cGAS^{FL}, or NLRX1^{FL} protein, NLRC3^{FL} and the known DNA-binding cGAS^{FL} bound to DNA in a dose-dependent manner, whereas NLRX1^{FL} did not (Figure 1F). These data indicate that NLRC3 can bind DNA.

The LRR Domain of NLRC3 Binds dsDNA

NLRC3 contains three domains, CARD, NBD, and LRR. HEK293T cells transfected with NLRC3 deletion mutants (Figure 2A) showed that biotinylated HSV-60 dsDNA co-precipitated with NLRC3^{FL}, NLRC3$^{NBD\text{-}LRR}$, and NLRC3^{LRR} but not NLRC3^{CARD}, NLRC3$^{CARD\text{-}NBD}$, or NLRC3^{NBD} (Figure 2B). These results suggest that the LRR domain is needed for dsDNA binding. We next expressed and isolated recombinant NLRC3^{NBD} and NLRC3^{LRR} from insect cells and assessed protein enrichment by Coomassie stain (Figures S2D and S2E). The results of streptavidin pull-downs showed that recombinant NLRC3^{FL} and NLRC3^{LRR}, but not NLRC3^{NBD}, proteins bound to biotinylated HSV-60 dsDNA (Figure 2C), confirming that the NLRC3 LRR domain alone can bind DNA.

To further probe the binding sites within the LRR domain, we built a homology model of human NLRC3 (Figure 2D) based on multiple structural templates, including mouse NLRC4 (PDB: 4KXF) and rabbit NOD2 (PDB: 5IRM) (Hu et al., 2013; Maekawa et al., 2016)

(Table S1), identified by the I-TASSER structure prediction server (Roy et al., 2010). LRR domains of NLRC3 aligned well with that of NLRC4 and NOD2. The majority of structural variances originated from differently orientated helical segments in the NBD (Figure 2D). Notably, the electrostatic potential surfaces of $NLRC3^{LRR}$ exhibited a continuous patch of positive charges (blue patch in Figure 2E) composed of 43 residues of lysine or arginine. In contrast, $NLRC4^{LRR}$, $NLRX1^{LRR}$, and $NOD2^{LRR}$ possessed more negative charges (red patch in Figure 2E). The positively charged surface constituted 74% of the solvent exposed area of $NLRC3^{LRR}$, more than the exposed areas of $NLRC4^{LRR}$, $NLRX1^{LRR}$, and $NOD2^{LRR}$ (35%, 44% and 38%, respectively) (Figure 2E, bottom). This increased positive charge most likely facilitated the interaction between NLRC3 and DNA. As a first step to delineate the region of LRRs that might interact with DNA, we used all-atom molecular dynamics (MD) simulation to predict the dominant binding-interface between NLRC3 and HSV dsDNA. The simulation predicted that LRRs 1–4 (colored purple in Figure 2F, left) would clasp onto the DNA strand of 60 bp and would mediate most of the interactions, whereas the last four LRRs (13–16) would play a minor role in this interaction (Figure 2F, left). The interactions between LRRs 5–8, LRRs 9–12, and DNA were minimal. HSV-15 dsDNA was predicted to interact with LRRs 1–4 but not LRRs 13–16, possibly because of its limited length (Figure 2F, right). To test these predictions experimentally, we deleted LRRs 1–4, LRRs 5–8, LRRs 9–12, or LRRs 13–16. Streptavidin pull-down demonstrated that deletion of LRRs 1–4 (ΔLRR1–4) abolished binding to HSV-60 and HSV-15 dsDNA, and ΔLRR13–16 modestly affected interaction with HSV-60 (Figures 2G and 2H).

NLRC3 Binds to DNA with High Affinity

To more definitely define NLRC3 binding to DNA, we used Bio-Rad surface plasmon resonance (SPR). Recombinant $NLRC3^{FL}$ and $NLRC3^{LRR}$ proteins showed a dose-dependent resonance signal and rapid association with chip-immobilized dsDNA. It also showed weaker binding to dsRNA. The equilibrium dissociation constants (K_D) between NLRC3 and HSV-60 dsDNA or dsRNA were 3 and 25 nM, respectively (Figure 3A), suggesting that $NLRC3^{FL}$ binds to dsDNA eight times more strongly than dsRNA. In separate experiments, we showed that NLRC3 also bound to single-strand DNA (ssDNA) and DNA-RNA hybrids (Figure 3B). Conversely, a different NLR, $NLRX1^{FL}$, served as a specificity control. It did not bind to HSV-60 dsDNA but bound to 60 bp dsRNA, confirming its RNA-binding activity (Hong et al., 2012; Lu et al., 2015) (Figure 3C). Binding affinities of $NLRC3^{LRR}$ with HSV-60 dsDNA or dsRNA were 65 and 490 nM (Figure 3D), indicating that the LRR alone binds dsDNA 8 times more strongly than dsRNA, but its binding to dsDNA is weaker than that of the full-length protein. Consistent with earlier results, $NLRC3^{LRR}$ does not bind to LPS (Figure 3D). Streptavidin pull-down of bio-tinylated-dsDNA or -dsRNA with recombinant $NLRC3^{FL}$ or $NLRC3^{LRR}$ confirmed that $NLRC3^{FL}$ and $NLRC3^{LRR}$ proteins preferentially bind DNA over RNA (Figure 3E). The affinity of the catalytic domain of the mouse cGAS protein to bind to dsDNA is reported to be 20,000 nM (Li et al., 2013), and the affinity of the full-length human cGAS protein to bind to dsDNA is 87 nM (Kranzusch et al., 2013), whereas the hematopoietic expression, interferon-inducible nature, and nuclear localization (HIN) domain of AIM2 binding to dsDNA is 50 nM. (Jin et al., 2012). When we compared data across different reports (which has its inherent caveats), $NLRC3^{FL}$ displayed a higher affinity than $cGAS^{FL}$, whereas $NLRC3^{LRR}$ exhibited a similar

binding affinity as AIM2 HIN and higher affinity than the cGAS catalytic domain. Finally, we noted that full-length rNLRC3 bound dsDNA with higher affinity than rNLRC3^{LRR} (Figures 3A and 3D). A possible explanation for this is that the NBD region that contains the conserved Walker A and B ATPase (WA/WB) motifs might allosterically affect DNA binding. To assess this, we tested DNA binding by NLRC3 and NLRC3 with mutated WA/WB that is known to disrupt ATPase activity (Duncan et al., 2007), and the latter showed less association with HSV-60 dsDNA (Figure 3F).

DNA Ligand Binding to NLRC3 Enhances ATPase Activity and Unleashes STING and TBK1

Previous work in intact cells demonstrated that NLRC3 binds STING and inhibits its trafficking and activation (Zhang et al., 2014). To explore the role of dsDNA binding on NLRC3-STING association, we transfected HSV-60 dsDNA into HEK293T cells and found that it reduced the association of Flag-STING with HA-NLRC3^{FL} in a dose-dependent manner (Figure 4A). To test this with recombinant proteins, we purified recombinant STING$^{155-341}$ and two controls, ASC^{PYD} and cGAS (Figures S2F and S2G). Recombinant NLRC3 bound to recombinant STING$^{155-341}$, but not to ASC^{PYD} or cGAS (Figure S2H), and DNA disrupted NLRC3^{FL}-STING$^{155-341}$ interaction in a dose-dependent fashion (Figure 4B). To provide a physiological context, we showed that WT HSV-1 infection also relieved STING sequestration by NLRC3 in a multiplicity of infection (MOI)-dependent manner in HeLa cells (Figure 4C). Reduction of STING expression upon HSV-1 infection has been reported, but this does not occur with WT virus infection of HeLa cells (Kalamvoki and Roizman, 2014), as we showed in this experiment. To explore whether another NLRC3-interacting protein can be released by DNA binding to NLRC3, we analyzed the interaction of NLRC3 with TBK1, which was previously reported (Zhang et al., 2014). Recombinant NLRC3 interacted with recombinant TBK1 and the interaction was disrupted by HSV-60 DNA in a dose-dependent fashion (Figure 4D). Given that a previous paper showed NLRC3 association with ASC (Eren et al., 2017), we determined whether NLRC3 played a role in inflammasome priming and activation. WT and *Nlrc3*$^{-/-}$ bone-marrow-derived macrophages (BMDMs) were stimulated with LPS, and no difference in pro-IL-1β protein level was found in cell lysate subjected to western blot analysis (Figure S2I). No difference in IL-1β secretion was observed when WT and *Nlrc3*$^{-/-}$ BMDMs were treated with canonical NLRP3 inflammasome agonists such as ATP, nigericin, silica, or Alum after LPS-induced priming (Figure S2J, left). We were not able to detect noticeable IL-1β secretion in HSV-1-infected BMDMs; therefore, we were not able to test whether NLRC3 affected inflammasomes in response to infection with the virus (Figure S2J, right).

Although previous work shows that NLRC3 NBD interacts with STING (Zhang et al., 2014), our report revealed that the LRR domain was required for dsDNA binding. We explored whether DNA binding to LRR released STING. Constructs expressing proteins with the NBD domain all bound STING in HEK293T cells. However, the reduction of the NLRC3-STING interaction by HSV-60 DNA was observed only when the DNA-binding LRR domain was intact (Figure 4E). This is consistent with a model where DNA binding to LRR leads NLRC3 to dissociate from STING. To exclude the possibility that STING-binding to DNA was a factor in this experiment, we used gel filtration and SPR to reveal that

recombinant STING$^{155-341}$ did not bind to HSV-60 dsDNA but did bind to 2′ and 3′ cGAMP as a positive control (Figures S3A–S3C).

To assess the proposed dsDNA-based disruption of an NLRC3-STING interaction in intact cells, we performed microscopic co-localization analysis. We hypothesized that the presence of HSV-60 dsDNA would reduce the co-localization of NLRC3 and STING, and that this effect would depend on the ability of NLRC3 to bind dsDNA. To test this, we transduced HeLa cells with tetracycline-inducible lentiviruses expressing NLRC3–3xFlag and/or STING-HA and stably selected them. Stable cells were treated for 18 h with doxycycline to induce expression of epitope-tagged NLRC3 and STING and subsequently transfected with Cy5-labeled dsDNA or left untransfected for 6 hr. Cells were processed for immunofluorescence and subjected to confocal analysis and image processing. The percentage of NLRC3 co-localizing with STING decreased from a median of 42% in the absence of HSV-60 to 26% in its presence (n = 40 z stacks per condition) (Figures 4F and 4G). In contrast, there was no significant effect of dsDNA on NLRC3 and STING co-localization when the NLRC3 DNA-binding domain (LRRs 1–16) was removed (Figures 4H and 4I). These results support the idea that dsDNA binding to NLRC3 liberates STING in cells. This suggests that dsDNA binding to LRRs might affect the NBD domain, which binds STING. Given that the NBD encodes an ATPase domain that is important for the function of other NLRs, we tested whether DNA binding might affect ATPase activity. NLRC3 exhibited weak ATPase activity, whereas the addition of HSV-60 DNA caused a ~10-fold increase in ATP hydrolysis (Figure 4J). Comparing the structural models of NLRC3 alone versus NLRC3-HSV-60 complex also suggests that DNA binding to NLRC3^{LRR} induced conformational change in the NLRC3^{NBD}, especially around the WA/WB region (Figures S4A–S4C). To test whether the ATPase activity of NBD affects sequestration of STING by NLRC3, we tested the WA/WB mutant and showed that it failed to release STING when DNA was added (Figure 4K). Collectively, these data suggest a model where viral DNA ligand binds to NLRC3 and increases its ATPase activity, which is needed to facilitate its release of STING and TBK1.

DISCUSSION

NLRs are the largest family of intracellular innate immune receptors and serve divergent functions in the regulation of innate immunity. Although the best-known NLRs exhibit positive function in inflammatory and immune activation during infection and inflammation, this report focuses on a member of an unusual sub-group of NLRs, defined as inhibitory NLRs, which inhibit inflammatory responses. However, there is much debate as to whether these inhibitory NLRs are modulators rather than receptors, given that the ligands for most inhibitory NLRs are undefined. Interestingly, two groups have shown that the LRR domain of NLRX1 can bind RNA (Hong et al., 2012; Lu et al., 2015), although the functional consequence of this finding is unclear. Here, we show that NLRC3 is a DNA-binding protein that directly binds to dsDNA from a DNA virus with high affinity. The binding is mediated by the LRR domain, which contains a series of continuous patches of positive charges. This is consistent with a previous study showing that the electrostatic potential surfaces of the LRR of NLRX1 also accommodate RNA molecules (Hong et al., 2012). Recently, LTA, a molecule produced by Gram-positive bacteria, has been reported to bind to NLRP6 via the

LRR domain and activate the NLRP6 infammasome (Hara et al., 2018). Another group showed that ASC immunoprecipitated with NLRP3 and mitochondrial DNA (mtDNA) when BMDMs were treated with ATP and nigericin after LPS-induced priming (Zhong et al., 2018). However, this study did not determine whether NLRP3 directly binds to mtDNA. In contrast to ligand binding to NLRs that exhibit a positive regulatory function, our findings demonstrate that a viral PAMP represented by dsDNA engages an inhibitory NLR to alter its function. These findings are in line with the ligand binding capacity of the LRR domain of Tolllike receptors (TLRs) and suggest an evolutionarily conserved function of LRR across multiple pattern-recognition receptors (PRRs).

Although most innate immune receptors are activated by PAMPs, our work demonstrates a paradigm where the viral DNA ligand binding to NLRC3 releases its binding to STING, thus liberating STING to activate the interferon pathway. In addition to STING, TBK1 is another NLRC3-associated protein kinase that phosphorylates STING and the transcription factor interferon regulatory factor 3 (IRF3) to induce type I interferon. This study shows that DNA binding to NLRC3 also releases its interaction with TBK1 in a cell free system. Because of the high-affinity binding between NLRC3 and dsDNA, it is possible that this binding could liberate other NLRC3-associated proteins described in the literature, such as TNF-receptor-associated factor 6 (TRAF6) and Ras GTPase-activating-like protein IQGAP1 (Schneider et al., 2012b; Tocker et al., 2017). Given that inhibitory NLRs function as checkpoints that prevent excessive immune responses, it would be interesting to determine whether nucleic acid binding to NLRC3 casts a suppressive effect on other downstream pathways such as Lys63 (K63)-linked ubiquitination of TRAF6 and phosphoinositide 3-kinases (PI3Ks) (Karki et al., 2016; Schneider et al., 2012b). NLR family members are defined by a central NBD that contains the highly conserved Walker A and Walker B motifs. The function of this domain is to bind and hydrolyze ATP, which we and others demonstrated by using purified NLRP3, NLRP12, NOD2, and NLRC4 proteins (Duncan et al., 2007; Hu et al., 2013; Mo et al., 2012; Ye et al., 2008). In this report, binding of DNA to the NLRC3 LRR allosterically enhances ATPase activity encoded within the NBD by 10-fold. Intact ATPase activity is required for NLRC3 to release STING and abrogation of ATPase activity by mutation of the Walker A/B motifs reduces STING release. It will be of interst to test whether the Walker A or Walker B motif is more critical or do these two motifs cooperatively contribute to DNA binding or STING release. Eventually, the precise molecular mechanism would greatly benefit from atomic resolution structures of NLRC3-HSV-60 and NLRC3-STING complexes.

To date, no viral ligands have been found for inhibitory NLRs. This report employed multiple approaches to demonstrate that dsDNA is a ligand for NLRC3 and unveiled a previously unappreciated mechanism by which the host uses viral DNA and most likely other forms of cytosolic nucleic acids to restrict the inhibitory function of NLRC3, causing it to liberate key signaling molecules such as STING and TBK-1. It is possible that NLRC3 might also have other functions including positive regulatory functions that have yet to be found, and it will be of interest to decipher whether DNA ligand binding also affects these other functions.

STAR★METHODS

CONTACT FOR REAGENT AND RESOURCE SHARING

Further information and requests for resources and reagents should be directed to and will be fulfilled by the Lead Contact, Jenny P.-Y. Ting (jenny_ting@med.unc.edu).

METHOD DETAILS

Mice

All studies were conducted in accordance with IACUC guidelines of UNC Chapel Hill and the NIH guide for the Care and Use of Laboratory Animals. *Nlrc3*$^{-/-}$ mice have been described previously (Zhang et al., 2014). WT and *Nlrc3*$^{-/-}$ mice in this study were generated from common *Nlrc3*$^{+/-}$ parents, which were obtained from at least 9 generations backcross to WT C57BL/6J mice, and were bred in house for several generations. All experiments used littermate controls, or their immediate descendants.

Cell Culture

HEK293T and HeLa cells were purchased from ATCC, and were maintained in DMEM supplemented with 10% FBS, 1% penicillin, 100ug/mL streptomycin, 1 mM sodium pyruvate, 2mM L-Glutamine, and 0.1mM nonessential amino acids. *Nlrc3*$^{+/+}$ and littermate control *Nlrc3*$^{-/-}$ MEFs were generated from 13.5-day embryos and maintained in complete DMEM medium as described above. All cells were grown at 37°C and 5% CO_2.

Plasmids, reagents and antibodies

HA-tagged NLRC3, NLRX1, STING, domain truncated NLRC3 and FLAG-tagged STING, NLRC3, RIG-I plasmids have been described (Moore et al., 2008; Zhang et al., 2014). Four LRR domain mutants of HA-NLRC3 (ΔLRR1 −4, ΔLRR5–8, ΔLRR9-12, and ΔLRR13-16) were engineered into pCDNA3.1 using Phusion mutagenesis (Thermofisher, Waltham, MA, USA) according to the manufacturer's instructions. Primers include: ΔLRR1-4: 5′ PHOS GCTTTGAAGATCAACCGCACCCTGACCTCCC and CATGGCCTCCTCCACGCTGCGGG, ΔLRR5-8: 5′ PHOS GCCCTCTGCACCAACCAGACCCTCCTCAGC and GTCTGCCAGCGCCTTGGCCCCTTG, ΔLRR9-12: 5′ PHOS GCACTGAAGGTCAACACAGCCCTCACTGCTCTCTATCTCC and CCCCATCAGTGCTGCCACTCCTGCG, and ΔLRR13-16: 5′ PHOS GCCATCAAGACAAATGCTCCCACGTGC and ACGGGCCACCGCACACGC. The template vector pCIG2-PURO-hNLRC3-3×Flag was generated using traditional cloning methods. Briefly: two primers encoding a glycine linker and a 3×-Flag tag (GGGGDYKDDDDKGADYKDDDDKEFDYKDDDDK) were annealed and extended to generate a dsDNA fragment(GCTCCCACGTGCACTGTTGAAATGGGCGGTGGCGGTGATTATAAAGATG ATGATGATAAAGGGGCAGACTACAAGG and ATATGGATCCTCACTTGTCGTCGTCGTCCTTGTAGTCGAATTCCTTGTCGTCGTCGT CCTTGTAGTCTGCCCCTTTATC), which served as the reverse primer for the PCR amplification with an NLRC3 forward primer

(GGGGGATATCACCATGAGGAAGCAAGAGGTGCGGACG) using pCDNA3.1-HA-hNLRC3 (Zhang et al.,2014) as template. The 3×-Flag tagged NLRC3 amplicon was cloned into the EcoRV/BamHI site of pCIG2-IRES-PURO, a variant of pCIG2-IRES-eGFP (Petrucelli et al., 2012). The pInducer20-NLRC3–3×Flag was constructed using the Gateway cloning system (Thermofisher). Briefly, NLRC3-3×Flag from pCIG2-PURO-hNLRC3-3×Flag was TA cloned into the entry vector, pENTR/D-TOPO (Thermofisher) using two primers CACCATGAGGAAGCAAGAGGTGCGGACG and TCATCACTTGTCGTCGTCGTCCTTGTAGTCG. The NLRC3-3×Flag insert was subsequently cloned into the tetracyline inducible destination vector pInducer20 (a kind gift of Bernard Weissman, The University of North Carolina at Chapel Hill, Chapel Hill, NC, USA) according to the manufacturer's LR Cloning protocol (Thermofisher). pInducer20-NLRC3-ΔLRR was generated through Phusion Mutagensis (Thermofisher) of pENTR/D-TOPO-NLRC3-3×Flag using two primers CATGGCCTCCTCCACGCTGCGGG and 5′ PHOS GCCATCAAGACAAATGCTCCCACGTGC followed by LR cloning (Thermofisher) into pInducer20 according to the manufacturer's instructions. All NLRC3 constructs were sequenced using a combination of vector specific and NLRC3 specific sequencing primers including: NLRC3 specific sequencing primers, CGGCAAGGACTTCTCGCTGG, TCACGGGGATGGCGCTAGGC, GAGGGAGGCCAGCCTGTGCC, CGGGCCATGCAGGCAGAGG, CATTCAGAAGATCAGCTTGGCGG, AGACCCTCCTCAGCCTCAGCC, GGTGGCTGGAGCCAAAGCCC, pCIG2-IRES-PURO sequencing primers GGGAGGTCTATATAAGCAGAGCTCGTTTA and GCCAAAAGACGGCAATATGGTGGAAAAT, pENTR/D-TOPO sequencing primers CACGACGTTGTAAAACGACGGCC and AGCTGCCAGGAAACAGCTATGACC, pInducer20 sequencing primers, AGCTCGTTTAGTGAACCGTCAGATC, CCCCTACCCGGTAGAATTTCTAG. pUNO1-hcGAS-FLAG was a kind gift from Blossom Damania (UNC-CH). pCW-hSTING-HA was a kind gift of Dr. Stanley Lemon (UNC-CH). Lentiviruses expressing NLRC3-3×Flag and STING-HA were generated as described previously (Petrucelli et al., 2012). HA-DDX41 and HA-IFI16 was a kind gift of Dr. Yongjun Liu (Sonofi, Paris, France). All primers including the biotinylated HSV60 was synthesized from Integrated DNA Technologies (Coralville, Iowa, USA). Un-biotinylated HSV60 DNA and 2′3′ cGAMP was purchased from InvivoGen (San Diego, CA, USA). Anti-NLRC3 (398947) was from Santa Cruz (Santa Cruz, CA, USA), and anti-HA(3724,), anti-FLAG (14793) antibodies (Western blot only) were from Cell Signaling Technologies (Danvers, MA, USA). Anti-Halo tag antibody (G9211) was from Promega (Madison, WI, USA) and anti-His tag antibody (A00186-100) was from GenScript (Piscataway, NJ, USA).

Cell stimulation and virus infection

MEFs were plated in 24-well plates and grown to 80% confluence overnight. MEFs were infected with HSV-1 (KOS strain) at MOI of 10 at 37°Cfor 1 hour. Cells were then washed with warm PBS and cultured in complete DMEM. Wild-type (WT) and *Nlrc3*$^{-/-}$ BMDMs were stimulated with LPS (300 ng/mL) at different time points (0, 2h, 4h and 6h), and pro-IL-1β protein expression in cell lysate was tested by western blot. Anti-Mouse-IL-1β was purchased from RD System (AF-401-NA). For NLRP3 inflammasome activation assays, wild-type (WT) and *Nlrc3*$^{-/-}$ BMDMs were primed with LPS (300 ng/mL) for 3 h and activated with canonical NLRP3 inflammasome agonists including ATP (10 mM), Nigericin

(20 μM), Silica and Alum (300 ug/mL) for 3 h. For HSV-1 infection, wild-type (WT) and *Nlrc3*$^{-/-}$ BMDMs were challenged by HSV-1 virus at different multiplicity of infection (MOI = 10 and 50) for 1h, 3h, 6h and 9h. Secreted IL-1β was examined by Mouse IL-1β ELISA kit (Biolegend, 432601).

Real time RT-PCR

Total RNA was extracted by TRIzol reagent (Thermofisher) and real-time PCR was performed using Power SYBR Green Master Mix (Thermofisher) on an ABI7900 cycler (Applied Biosystems). Please see the primers in Table S2.

Pulldown assay

To assay DNA binding to HA-tagged NLRC3 in cell lysate, 293T cells were transfected with indicated plasmids. After 24 hours, 293T cells were washed twice, collected and lysed in buffer containing 50 mM Tris-HCl, 150 mM NaCl, 1% NP-40, and 5 mM EDTA, protease inhibitor cocktail and phosphatase inhibitor cocktail (Roche, Basel, Switzerland) for 30 min. Cell debris was pelleted by centrifugation at 16,000 × g for 15 min at 4°C. 2 μg of biotin-conjugated dsHSV60 or LPS were first immobilized onto 15 mL of streptavidin Sepharose beads. The beads were washed three times with lysis buffer (described above) to remove unconjugated ligands, and were then added to pre-cleared lysates to perform the standard pulldown assay. For the competition assay, the pre-cleared lysates were first incubated with 5 μg or 20 μg of unlabelled dsHSV60 or LPS for 2 hours at 4°C with constant rotation, then added to biotinylated HSV60-conjugated streptavidin beads to perform the standard pulldown assay. To assay if DNA alters NLRC3 binding with STING, 293T cells were transfected with the indicated plasmids for 24 hours, followed by transfection with 1 μg or 4 μg dsHSV60 for 6 hours. Anti-HA agarose beads (E6779, Sigma) was used to perform the pulldown assay. For Herpes simplex virus 1 (HSV-1) infection immunoprecipitation assay, HeLa cells co-expressing NLRC3-3×Flag and STING-HA was treated for 18 hours with 2 μg/mL doxycycline to induce expression of epitope-tagged NLRC3 and STING, and subsequently infected with Herpes simplex virus 1 (HSV-1) for 6 hours (MOI = 10 and 100).

ATPase assay

ATPase assays were conducted by previously described (Duncan et al., 2007) with modification. The reaction was initated by adding NLRC3 protein into the reaction mixture consisting of 125 nM [γ-33-ATP], 10 μM unlabeled ATP, 50 mM Tris-HCl (pH 7.5), 150 mM NaCl, 0.5 mM TECP, 2.5 mM $MgCl_2$ and 5% glycerol with and without 100 nM HSV60 DNA. The reaction was performed at 30°C. At the indicated time points, 100 μL of the reaction was removed and added to 500 μL of acidified charcoal (30% charcoal Norit in 100 mM HCl and 100 mM Na_2HPO4). The charcoal was spun down by centrifugation at 13,000 rpm for 5 min, and 100 μL of supernatant containing free ^{33}P-PO4 was counted by scintillation counter.

Confocal microscopy

HeLa cells were transduced with lentiviruses expressing NLRC3-3×Flag and STING-HA in the presence of 8 μg/mL polybrene (H9268) (Sigma, St. Louis, MO, USA). The growth

media was replaced 24 hours post transduction. After 48 hours of transduction, cells were treated with puromycin (P8833, Sigma) (1.0 μg/mL selection for pCW vector) or G418 (10131035, Thermofisher) (750 μg/mL selection for pInducer20 vector) or both for 14 days prior to use in experiments. HeLa cells (7.5×10^4) were seeded onto No. 1.5 glass coverslips (Thermofisher) in 24 well dishes. STING-HA and NLRC3-Flag expression were induced with 0.25 ug/mL doxycycline hyclate (Sigma D9891) 18 hours prior to transfection with dsDNA. Cells were transfected with Cy5 labeled HSV-60 dsDNA (IDT) (500 ng/well) for 6 hours using Lipofectamine 2000 (Thermofisher) according to the manufacturer's instructions. Cells were washed in phosphate-buffered saline (PBS), fixed in 2% paraformaldehyde in PBS at room temperature for 20 min, and permeabilized with 0.1% Triton X-100 in PBS at room temperature for 10 min. Cells were then blocked in PBS containing 2.5 mg/mL BSA and 1% normal goat serum for 30 min at 4°C. Primary antibodies include mouse anti-HA (HA-7, H3663, Sigma) and rabbit anti-Flag (F7425 Sigma), both used at 1:200 in blocking buffer for 1 hour at room temperature. Cells were washed with PBS plus 0.05% Tween 20, 4 times for 3 min each. Secondary antibodies conjugated to fluorescent molecules included Alexa Fluor 546-conjugated goat anti-mouse IgG (H+L) (A-11003) and Alexa Fluor 488-conjugated goat anti-rabbit IgG (H+L) (A-11008) (Invitrogen, Carlsbad, CA, USA). Secondary antibodies were applied in blocking buffer for 1 hour at room temperature. Cells were washed with PBS plus 0.05% Tween 20, 4 times for 3 min each, and incubated in 1 μg/mL DAPI (4′,6′-diamidino-2-phenylindole) in PBS for 5 min at room temperature. Coverslips were mounted on slides with Aqua Polymount (Polysciences, Inc, Warrington, PA, USA) and visualized using a Zeiss LSM700 confocal microscope (Carl Zeiss Microimaging, Inc. Thornwood, NY, USA) using a 63×/1.4 Plan Apochromat Oil DIC objective. Z stacks were acquired with the following settings: Pinhole = 1 AU for the longest wavelength (Cy5), 12 bit, 512 × 512, 0.14 μm pixel size, with Z-slices spaced at 0.4 μm intervals. Image stacks were acquired with 4 separate tracks run in the following order, Cy5, AF546, AF488, and DAPI. Channel Pinhole settings: Cy5 = 54.76 μm, AF546 = 48.29 μm, AF488 = 48.29 μm, DAPI = 48.29 μm. Channels were crosschecked for bleed-through using individualy stained color controls. Image stacks were processed as follows: Images were deconvolved using the default blind 3D deconvolution settings in the Autoquant 3 software suite (Media Cybernetics) and image stacks exported as bitplane, tiff, and LSM files. Z axis profiles were plotted for each channel to attain the maximal signal containing slice in FIJI (Schindelin et al., 2012; Schneider et al., 2012a). Slices displaying maximum intensity for each stack were selected and a new stack of maximal slices for each channel was created. All image stacks for a given channel were concatenated into a large stack of maximal slices for all images in each channel. Concatenated stacks were assembled into montages for each channel. Thresholds were set for each channel by visually evaluating these montages (For NLRC3 analysis: Cy5 dsDNA = 24, AF546 STING-HA = 40, AF488 NLRC3-3×FLAG = 114, DAPI Nucleus = Auto, For NLRC3 ΔLRR1-16: Cy5 dsDNA = 24, AF546 STING-HA = 20, AF488 NLRC3-3×FLAG = 92, DAPI Nucleus = Auto). Thresholds were subsequently used for co-localization analysis using the Co-Loc package in Imaris software (Bitplane). 3D Co-localization analysis was performed and individual channel and co-localizing voxel maps (3D surfaces) were generated in Imaris using the previously determined threshold settings. For visual representation, 3D surfaces of each channel from representative images are displayed (with varying degrees of transparency)

with the DAPI surface. Microscopy and analysis was performed at the UNC-CH Microscopy Services Laboratory at UNC-CH (UNC-CH Chapel Hill, NC, USA). N = 40 z stacks for each experimental condition (+/− DNA). Statistical analysis was performed in GraphPad Prism software (GraphPad, La Jolla, CA, USA) using 2-tailed Student's t tests. P values are indicated.

NLRC3/HSV60 DNA gel shift assay

Aliquots of NLRC3, cGAS and NLRX1 recombinant protein (1 μg, 2 μg, 3 μg, 4 μg, 5 μg in 50 mM Tris-HCl pH 7.5, 150 mM NaCl, 0.1% CHAPS, 1mM DTT) were mixed with 1 pmol of biotinylated HSV60 dsDNA and incubated at room temperature for 30 min. Controls included, protein only and biotinylated-HSV60 only reactions. After incubation for 30 min, proteins and biotinylated HSV60 DNA were crosslinked with 1% formaldehyde for 30 min on ice. Crosslinking was quenched by adding glycine to a final concentration of 125 mM. Reactions were subjected to gel electrophoresis (6% Novex DNA Retardation gel, Invitrogen, Carlsbad, CA, USA) and transferred to nylon membranes (Nytran Supercharge nylon membrane, Schleicher and Schuell, Dassel, Germany). Biotin-labeled DNA was detected using the Lightshift Chemiluminescent EMSA kit (Thermofisher).

Recombinant Protein purification and *in vitro* co-immunoprecipitation assays

N-terminal Halo-Tag (Halo) and C-terminal hexahistidine tag (6xHis) recombinant human NLRC3 full-length, NLRX1 full-length, NLRC3-NBD and NLRC3-LRR proteins were expressed in baculovirus infected insect cells as described previously (Mo et al., 2012). Mouse full-length cGAS and human STING (residues 255-341) was cloned into N-terminal His-SUMO tagged pET-28 (a) vector. Human ASC^{PYD} (residues1-106) was cloned into pDB-His-MBP vector. All the cGAS, STING and ASC constructs were transformed and expressed in *E.coli* BL21(DE3) at 15°C and purified as described previously (Li et al., 2013). 1 pmol of biotinylated HSV60 DNA (IDT) was incubated with 3 μg Halo-tagged protein and added to IP buffer containing 50 mM Tri-HCl, 150 mM NaCl, 1 mM DTT and 0.1% CHAPS. After 4 hours rotating at 4°C, streptavidin magnetic resin was added to each reaction and rotated for 1 hour. The biotinylated-resin-associated proteins were isolated by centrifugation at 6,000 × g for 30 s at 4°C and the resins were washed four times with buffer (50 mM Tris-HCl, 300 mM NaCl, 1 mM DTT and 0.1% CHAPS). The proteins were resolved on SDS-PAGE gels, and analyzed by immunoblot. For DNA releasing assays, purified NLRC3 (1μg), purified $STING^{155-341}$ (1μg) or 1μg recombinant human TBK1 protein (A31514, Thermo-Fisher) and titrations of HSV60 DNA were mixed in IP buffer. After 4 hours rotating at 4°C, Halolink resin (G1914, Promega) was added into each reaction for 1 hour. The Halo-resin-associated proteins were isolated by centrifugation at 6,000 × g for 30 s at 4°C and the resin was washed with IP buffer containing 300 mM NaCl and detected by immunoblot.

Surface plasmon resonance (SPR)

Analyses of ligand binding and binding kinetics were performed at 25°C on a ProteON™XPR36 Protein Interaction Array System (Bio-Rad Laboratory, Hercules, CA, USA). Running buffer consisted of 20 mM Tris-HCl (pH7.5), 150 mM NaCl, 100 μM TCEP, and 0.005% (v/v) Tween-20. The blocking buffer consisted of 0.1% BSA in running buffer.

Biotinylated HSV60 DNA, HSV60 RNA, HSV60 ssDNA, HSV60 DNA-RNA hybrids (50 nM) or LPS (40nM) ligand was loaded on an NLC sensor chip (Bio-Rad) for 1 min. After flowing the ligand, the NLC sensor chip was blocked for 30 min. Recombinant NLRC3, NLRX1, $NLRC3^{LRR}$ (0.1 μM, 0.3 μM, 1 μM), and $STNG^{155-341}$ (10 μM, 15 μM, 30 μM) proteins were loaded on the sensor chip at a flow rate of 100 μl/min for 2 min and dissociated for 5 min. The resulting data were analyzed by fitting to a 1:1 Langumir binding model using the Bio-Rad ProteON-XPR36 evaluation software by subtracting the control values.

Protein structural modeling

The structural model of human NLRC3 was generated using the homology modeling module of the I-TASSER webserver (http://zhanglab.ccmb.med.umich.edu/I-TASSER) (Roy et al., 2010). Multiple structural templates were identified by the multi-thread module LOMETS in I-TASSER, including NLRC4 (4KXF) and NOD2 (5IRM, 5IRL, 5IRN) proteins (Table S1). The templates were ranked by I-TASSER based on sequence identity, coverage and Z-score. Among them, the crystal structure of mouse NLRC4 (4KXF) was identifed as the top template and the sequence similarity between NLRC3 and NLRC4 is 34.1%, as determined by pairwise sequence alignment on the EMBOSS NEEDLE server. The default parameters were adopted in the I-TASSER calculation without additional constraints on any residues or specified secondary structure segments. This calculation generated five homology models and the model with the lowest free energy was chosen for further equilibration by molecular dynamics (MD) simulations under physiological conditions (200 ns simulation at 298K, 150 mM NaCl and neutral pH). After structural relaxation, the electrostatic potential surfaces of NLRC3, NLRC4 (PDB: 4KXF) (Hu et al., 2013), NOD2 (5IRM) (Maekawa et al., 2016) and NLRX1 (PDB: 3UN9) (Hong et al., 2012) were calculated with Adaptive Poisson-Boltzmann Solver (Jo et al., 2008).

For preparation of initial binding conformations of NLRC3-HSV60, we used HADDOCK2.2 following the procedure described by van Zundert et al. (van Zundert et al., 2016) and instructions on the website (https://haddock.science.uu.nl/services/HADDOCK2.2/). The MD simulations were performed on Gromacs 4.6.3 with all-atom resolutions (Hess et al., 2008). The force field CHARMM36 was adopted with the explicit solvent model TIP3P (Huang and MacKerell, 2013). The system was solvated and neutralized with 150 mM NaCl, constituting 19184 atoms for protein and DNA and ~101000 atoms for solvents and ions with the dimensions of 110 × 115 × 220 Å. The simulations were performed at 300 K (velocity-rescale thermostat) and constant pressure (1 bar, Parrinello-Rahman NPT ensemble). The non-bonded interaction cut-off for electrostatics calculations was set as 10 Å and the particle mesh Ewald (PME) method was used in the calculation of long-range electrostatic interactions. The system was minimized and equilibrated for 1 ns before the production run, which used periodic boundary conditions. No constraint was set on NLRC3 and harmonic force constraints were applied within the DNA base pairs to prevent the dissociation of the double-strand. Simulated annealing was applied to accelerate the sampling and a typical annealing procedure was: 0 ns 300 K - 5 ns 500 K - 20 ns 300 K - 40 ns 200 K. A 100-ns equilibrium simulation was performed to examine the stability of the modeled structure after simulated annealing. Throughout the

trajectories, the representative binding conformations were clustered based on their structural similarities. After reaching equilibrium, these conformations were extracted for further analysis.

DNA and RNA Sequences

HSV60 bp DNA: 5′-biotin-TAAGACACGATGCGATAAAATCTGTTTGTAAAATTTATT AAGGGTACAAATTGCCCTAGC-3′; 15bp DNA: 5′-biotin-TAAGACACGATGCGA-3′; 60bp RNA: 5′-biotin-UAAGACACGAUGCGAUAAAAUCUGUUUGUAAAAUUUAUUAAGGGUACAAAUU GCCCUAGC-3′; 15bp RNA: 5′-biotin-UAAGACACGAUGCGA-3′; HSV60 bp DNA: 5′-Cy5-TAAGACACGATGCGATAAAATCTGTTTGTAAAATTTATTAAGGGTACAAATTGCCC TAGC-3′; HSV60 ssDNA: 5′-biotin-TAAGACACGATGCGATAAAATCTGTTTGTAAAATTTATT AAGGGTACAAATTGCCCTAGC-3′; HSV60 hybrid DNA: forward 5′-biotin-TAAGACACGATGCGATAAAATCTGTTTGTAAAATTTATTAAGGGTACAAATTGCCC TAGC-3′, reverse RNA: 5′-GCUAGGGCAAUUUGUACCCUUAAUAAAUUUUACAAACAGAUUUUAUCGCAUCG UGUCUUA-3′.

RNA interference

HEK293T cells were transfected with NLRC3 plasmid and pLKO.1 shRNA for 24 h, then cells were used for streptavidin pulldown experiments. A shRNA clone containing *NLRC3* targeting sequence GCAACCTCTTTCCGGAAGTTT was acquired from Broad Institute (clone ID: TRCN0000168401). pLKO.1 GFP shRNA was used as a scramble control (Plasmid #30323, addgene).

IP-qPCR assay

HEK293T cells were transfected with pcDNA3.1, HA-NLRC3, or HA-NLRX1 plasmid for 24 hours followed by transfection of HSV60 dsDNAfor 6 hours. The cells were crosslinked with formaldehyde (1% final concentration) at room temperature for 10 min and the cross-link was quenched by adding glycine (0.125 M final concentration). Then the cells were washed with PBS and resuspended in Cell Lysis Buffer (10 mM Tris, 10 mM EDTA, 0.5 mM EGTA, 0.25% Triton X-100, 0.5% NP-40, pH 8.0) at 4°C for 15 min. The lysates were cleared by centrifugation at 12,000 × g for 20 min at 4 °C and then mixed with anti-HA antibody (3724, Cell Signaling) and Protein G beads (SureBeads Protein G Magnetic Beads, BIO-RAD) overnight at 4 °C. The precipitates were washed twice with Low Salt Immune ComplexWash Buffer (0.1% SDS,2 mM EDTA, 150mM NaCl, 20mM Tris-Cl, pH 8.0), then twice with HighSalt Immune Complex Wash Buffer (0.1% SDS, 1% Triton, 2 mM EDTA, 500 mM NaCl, 20 mM Tris-Cl, pH 8.0), and twice with LiCl Immune Complex Wash Buffer (0.25 M LiCl, 1% NP-40,1% Na deoxycholate, 1 mM EDTA, 10 mM Tris-Cl, pH 8.0). Protein bound DNA was eluted in Elution Buffer (1% SDS, 100 mM $NaHCO_3$) and the cross-links were reversed by adding 5M NaCl and incubating at 65°C overnight. The elution was then treated with RNase and Proteinase K. Then DNA was purified by phenol-chloroform extraction and analyzed using SYBR green based quantitative real-time PCR to

determine the relative enrichment of HSV60 dsDNA. The HSV dsDNA amount in input sample was used as internal control. Protease and phosphatase inhibitor cocktails were added into all lysis and wash buffer. Please see the primers in Table S2.

Statistical analysis

GraphPad Prism 6.0 software was used for data analysis. Data are shown as mean ± SEM. Statistical significance was determined by t test (two-tailed) for two groups. Multiple comparisons were analyzed by one-way ANOVA with Tukey's posttests. $p < 0.05$ was considered statistically significant.

DATA AND SOFTWARE AVAILABILITY

All data generated or analyzed during the study are included in this published article and are available from the corresponding author upon reasonable request.

Supplementary Material

Refer to Web version on PubMed Central for supplementary material.

ACKNOWLEDGMENTS

We thank Dr. Ashutosh Tripathy, Director of the Center for Structural Biology University of North Carolina (UNC) Macromolecular Interactions Facility, for providing core and technical support. We also thank William G. Fusco at UNC for assistance with the EMSA. This work was supported by NIH U19-AI109965 to J.P.-Y.T. and J.A.D and NIH R01AI029564 and U19-AI067798 to J.P.-Y.T. N.V.D. acknowledges NIH support grants R01GM114015 and R01GM123247. A.S.P. and J.W.T. were supported by T32CA009156.

REFERENCES

Bürckstümmer T, Baumann C, Blüml S, Dixit E, Dürnberger G, Jahn H, Planyavsky M, Bilban M, Colinge J, Bennett KL, and Superti-Furga G (2009). An orthogonal proteomic-genomic screen identifies AIM2 as a cytoplasmic DNA sensor for the inflammasome. Nat. Immunol. 10, 266–272. [PubMed: 19158679]

Chamaillard M, Hashimoto M, Horie Y, Masumoto J, Qiu S, Saab L, Ogura Y, Kawasaki A, Fukase K, Kusumoto S, et al. (2003). An essential role for NOD1 in host recognition of bacterial peptidoglycan containing diaminopimelic acid. Nat. Immunol. 4, 702–707. [PubMed: 12796777]

Conti BJ, Davis BK, Zhang J, O'connor W Jr., Williams KL, and Ting JP (2005). CATERPILLER 16.2 (CLR16.2), a novel NBD/LRR family member that negatively regulates T cell function. J. Biol. Chem. 280, 18375–18385. [PubMed: 15705585]

Duncan JA, Bergstralh DT, Wang Y, Willingham SB, Ye Z, Zimmermann AG, and Ting JP (2007). Cryopyrin/NALP3 binds ATP/ dATP, is an ATPase, and requires ATP binding to mediate inflammatory signaling. Proc. Natl. Acad. Sci. USA 104, 8041–8046. [PubMed: 17483456]

Elinav E, Strowig T, Kau AL, Henao-Mejia J, Thaiss CA, Booth CJ, Peaper DR, Bertin J, Eisenbarth SC, Gordon JI, and Flavell RA (2011). NLRP6 inflammasome regulates colonic microbial ecology and risk for colitis. Cell 145, 745–757. [PubMed: 21565393]

Eren E, Berber M, and Özören N (2017). NLRC3 protein inhibits inflammation by disrupting NALP3 inflammasome assembly via competition with the adaptor protein ASC for pro-caspase-1 binding. J. Biol. Chem. 292, 12691–12701. [PubMed: 28584053]

Fernandes-Alnemri T, Yu JW, Datta P, Wu J, and Alnemri ES (2009). AIM2 activates the inflammasome and cell death in response to cytoplasmic DNA. Nature 458, 509–513. [PubMed: 19158676]

Girardin SE, Boneca IG, Carneiro LA, Antignac A, Jéhanno M, Viala J, Tedin K, Taha MK, Labigne A, Zähringer U, et al. (2003a). Nod1 detects a unique muropeptide from gram-negative bacterial peptidoglycan. Science 800, 1584–1587.

Girardin SE, Travassos LH, Hervé M, Blanot D, Boneca IG, Philpott DJ, Sansonetti PJ, and Mengin-Lecreulx D (2003b). Peptidoglycan molecular requirements allowing detection by Nod1 and Nod2. J. Biol. Chem. 278, 41702–41708. [PubMed: 12871942]

Guo H, Callaway JB, and Ting JP (2015). Inflammasomes: mechanism of action, role in disease, and therapeutics. Nat. Med. 21, 677–687. [PubMed: 26121197]

Hara H, Seregin SS, Yang D, Fukase K, Chamaillard M, Alnemri ES, Inohara N, Chen GY, and Nunez G (2018). The NLRP6 inflammasome recognizes lipoteichoic acid and regulates gram-positive pathogen infection. Cell 175, 1651–1664.e14. [PubMed: 30392956]

Harton JA, Linhoff MW, Zhang J, and Ting JP (2002). Cutting edge: CATERPILLER: a large family of mammalian genes containing CARD, pyrin, nucleotide-binding, and leucine-rich repeat domains. J. Immunol. 169, 4088–4093. [PubMed: 12370334]

Hess B, Kutzner C, van der Spoel D, and Lindahl E (2008). GROMACS 4: Algorithms for Highly Efficient, Load-Balanced, and Scalable Molecular Simulation. J. Chem. Theory Comput. 4, 435–447. [PubMed: 26620784]

Hong M, Yoon SI, and Wilson IA (2012). Structure and functional characterization of the RNA-binding element of the NLRX1 innate immune modulator. Immunity 86, 337–347.

Hornung V, Ablasser A, Charrel-Dennis M, Bauernfeind F, Horvath G, Caffrey DR, Latz E, and Fitzgerald KA (2009). AIM2 recognizes cytosolic dsDNA and forms a caspase-1-activating inflammasome with ASC. Nature 458, 514–518. [PubMed: 19158675]

Hu Z, Yan C, Liu P, Huang Z, Ma R, Zhang C, Wang R, Zhang Y, Martinon F, Miao D, et al. (2013). Crystal structure of NLRC4 reveals its auto-inhibition mechanism. Science 341, 172–175. [PubMed: 23765277]

Hu S, Du X, Huang Y, Fu Y, Yang Y, Zhan X, He W, Wen Q, Zhou X, Zhou C, et al. (2018). NLRC3 negatively regulates CD4+ T cells and impacts protective immunity during Mycobacterium tuberculosis infection. PLoS Pathog. 14, e1007266. [PubMed: 30133544]

Huang J, and MacKerell AD Jr. (2013). CHARMM36 all-atom additive protein force field: validation based on comparison to NMR data. J. Comput. Chem. 34, 2135–2145. [PubMed: 23832629]

Jin T, Perry A, Jiang J, Smith P, Curry JA, Unterholzner L, Jiang Z, Horvath G, Rathinam VA, Johnstone RW, et al. (2012). Structures of the HIN domain:DNA complexes reveal ligand binding and activation mechanisms of the AIM2 inflammasome and IFI16 receptor. Immunity 36, 561–571. [PubMed: 22483801]

Jo S, Vargyas M, Vasko-Szedlar J, Roux B, and Im W (2008). PBEQ-Solver for online visualization of electrostatic potential of biomolecules. Nucleic Acids Res. 36, W270–5. [PubMed: 18508808]

Kalamvoki M, and Roizman B (2014). HSV-1 degrades, stabilizes, requires, or is stung by STING depending on ICP0, the US3 protein kinase, and cell derivation. Proc. Natl. Acad. Sci. USA 111, E611–E617. [PubMed: 24449861]

Karki R, Man SM, Malireddi RK, Kesavardhana S, Zhu Q, Burton AR, Sharma BR, Qi X, Pelletier S, Vogel P, et al. (2016). NLRC3 is an inhibitory sensor of PI3K-mTOR pathways in cancer. Nature. 10.1038/nature20597.

Kofoed EM, and Vance RE (2011). Innate immune recognition of bacterial ligands by NAIPs determines inflammasome specificity. Nature 477, 592–595. [PubMed: 21874021]

Kranzusch PJ, Lee AS, Berger JM, and Doudna JA (2013). Structure of human cGAS reveals a conserved family of second-messenger enzymes in innate immunity. Cell Rep. 3, 1362–1368. [PubMed: 23707061]

Li X, Shu C, Yi G, Chaton CT, Shelton CL, Diao J, Zuo X, Kao CC, Herr AB, and Li P (2013). Cyclic GMP-AMP synthase is activated by double-stranded DNA-induced oligomerization. Immunity 39, 1019–1031. [PubMed: 24332030]

Lu P, Hontecillas R, Abedi V, Kale S, Leber A, Heltzel C, Langowski M, Godfrey V, Philipson C, Tubau-Juni N, et al. (2015). Modeling-enabled characterization of novel NLRX1 ligands. PLoS ONE 10, e0145420. [PubMed: 26714018]

Maekawa S, Ohto U, Shibata T, Miyake K, and Shimizu T (2016). Crystal structure of NOD2 and its implications in human disease. Nat. Commun. 7, 11813. [PubMed: 27283905]

Mo J, Boyle JP, Howard CB, Monie TP, Davis BK, and Duncan JA (2012). Pathogen sensing by nucleotide-binding oligomerization domain-containing protein 2 (NOD2) is mediated by direct binding to muramyl dipeptide and ATP. J. Biol. Chem. 287, 23057–23067. [PubMed: 22549783]

Moore CB, Bergstralh DT, Duncan JA, Lei Y, Morrison TE, Zimmermann AG, Accavitti-Loper MA, Madden VJ, Sun L, Ye Z, et al. (2008). NLRX1 is a regulator of mitochondrial antiviral immunity. Nature 451, 573–577. [PubMed: 18200010]

Petrucelli A, Umashankar M, Zagallo P, Rak M, and Goodrum F (2012). Interactions between proteins encoded within the human cytomegalovirus UL133-UL138 locus. J. Virol. 86, 8653–8662. [PubMed: 22674978]

Roy A, Kucukural A, and Zhang Y (2010). I-TASSER: a unified platform for automated protein structure and function prediction. Nat. Protoc. 5, 725–738. [PubMed: 20360767]

Schindelin J,Arganda-Carreras I, Frise E, Kaynig V, Longair M, Pietzsch T, Preibisch S, Rueden C, Saalfeld S, Schmid B, et al. (2012). Fiji: an open-source platform for biological-image analysis. Nat. Methods 9, 676–682. [PubMed: 22743772]

Schneider CA, Rasband WS, and Eliceiri KW (2012a). NIH Image to ImageJ: 25 years of image analysis. Nat. Methods 9, 671–675. [PubMed: 22930834]

Schneider M, Zimmermann AG, Roberts RA, Zhang L, Swanson KV, Wen H, Davis BK, Allen IC, Holl EK, Ye Z, et al. (2012b). The innate immune sensor NLRC3 attenuates Toll-like receptor signaling via modification of the signaling adaptor TRAF6 and transcription factor NF-κB. Nat. Immunol. 13, 823–831. [PubMed: 22863753]

Shi J, Zhao Y, Wang Y, Gao W, Ding J, Li P, Hu L, and Shao F (2014). Inflammatory caspases are innate immune receptors for intracellular LPS. Nature 514, 187–192. [PubMed: 25119034]

Sun L, Wu J, Du F, Chen X, and Chen ZJ (2013). Cyclic GMP-AMP synthase is a cytosolic DNA sensor that activates the type I interferon pathway. Science 339, 786–791. [PubMed: 23258413]

Tocker AM, Durocher E, Jacob KD, Trieschman KE, Talento SM, Rechnitzer AA, Roberts DM, and Davis BK (2017). The scaffolding protein IQGAP1 interacts with NLRC3 and inhibits type I IFN production. J. Immunol. 199, 2896–2909. [PubMed: 28864474]

Uchimura T, Oyama Y, Deng M, Guo H, Wilson JE, Rampanelli E, Cook KD, Misumi I, Tan X, Chen L, et al. (2018). The innate immune sensor NLRC3 acts as a rheostat that fine-tunes t cell responses in infection and autoimmunity. Immunity 49, 1049–1061.e6. [PubMed: 30566882]

Unterholzner L, Keating SE, Baran M, Horan KA, Jensen SB, Sharma S, Sirois CM, Jin T, Latz E, Xiao TS, et al. (2010). IFI16 is an innate immune sensor for intracellular DNA. Nat. Immunol. 11, 997–1004. [PubMed: 20890285]

van Zundert GCP, Rodrigues JPGLM, Trellet M, Schmitz C, Kastritis PL, Karaca E, Melquiond ASJ, van Dijk M, de Vries SJ, and Bonvin AMJJ (2016). The HADDOCK2.2 web server: user-friendly integrative modeling of biomolecular complexes. J. Mol. Biol. 428, 720–725. [PubMed: 26410586]

Ye Z, Lich JD, Moore CB, Duncan JA, Williams KL, and Ting JP (2008). ATP binding by monarch-1/NLRP12 is critical for its inhibitory function. Mol. Cell. Biol. 28, 1841–1850. [PubMed: 18160710]

Zhang Z, Yuan B, Bao M, Lu N, Kim T, and Liu YJ (2011). The helicase DDX41 senses intracellular DNA mediated by the adaptor STING in dendritic cells. Nat. Immunol. 12, 959–965. [PubMed: 21892174]

Zhang L, Mo J, Swanson KV, Wen H, Petrucelli A, Gregory SM, Zhang Z, Schneider M, Jiang Y, Fitzgerald KA, et al. (2014). NLRC3, a member of the NLR family of proteins, is a negative regulator of innate immune signaling induced by the DNA sensor STING. Immunity 40, 329–341. [PubMed: 24560620]

Zhao Y, Yang J, Shi J, Gong YN, Lu Q, Xu H, Liu L, and Shao F (2011). The NLRC4 inflammasome receptors for bacterial flagellin and type III secretion apparatus. Nature 477, 596–600. [PubMed: 21918512]

Zhong Z, Liang S, Sanchez-Lopez E, He F, Shalapour S, Lin XJ, Wong J, Ding S, Seki E, Schnabl B, et al. (2018). New mitochondrial DNA synthesis enables NLRP3 inflammasome activation. Nature 560, 198–203. [PubMed: 30046112]

Highlights

- NLRC3 binds to herpes simplex virus dsDNA via the LRR domain with high affinity
- DNA binding to NLRC3 diminishes its interaction with STING and TBK1 to enhance IFN-I
- DNA binding to NLRC3 enhances ATPase activity
- The ATPase activity of NLRC3 is crucial for DNA-mediated dissociation of STING

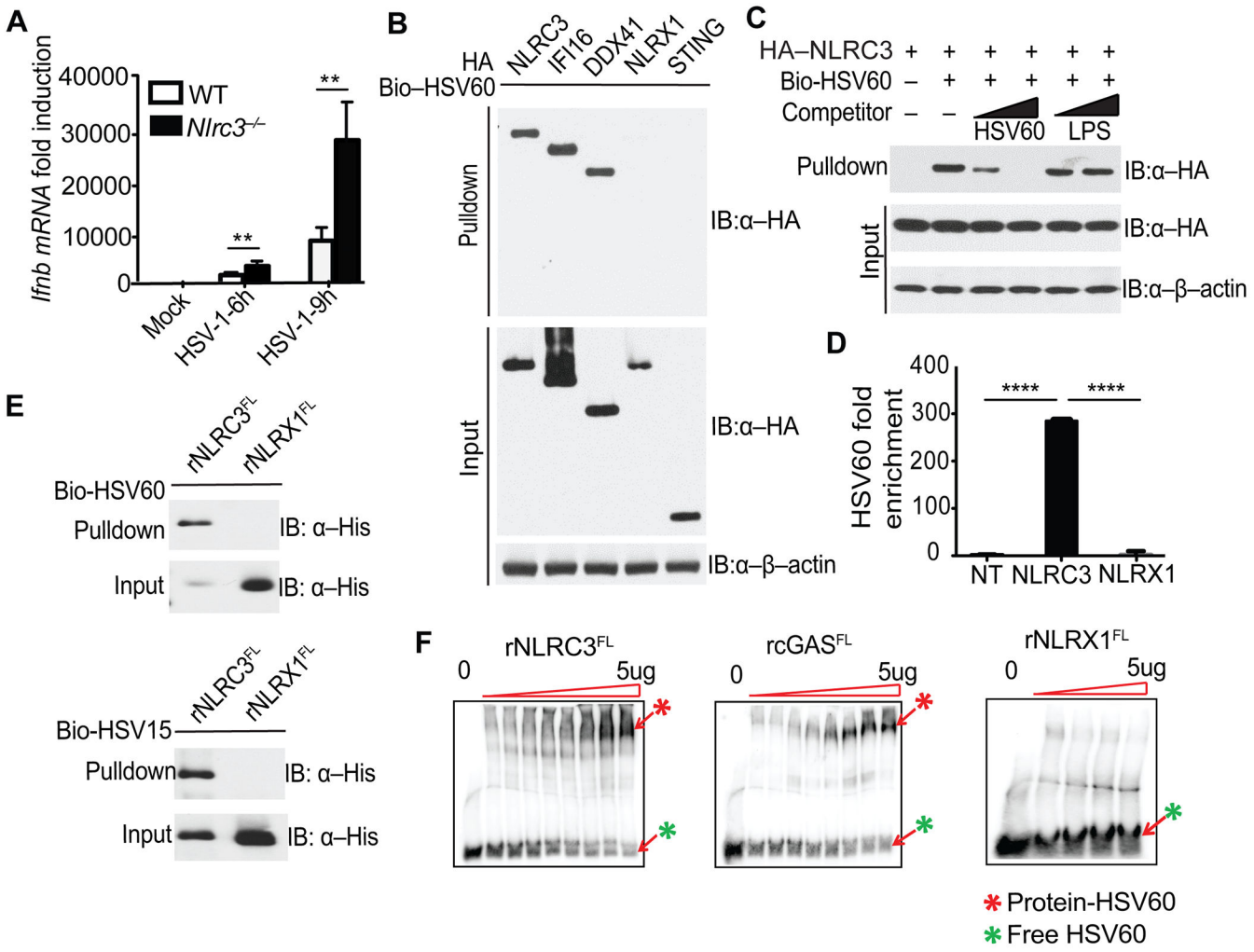

Figure 1. NLRC3 Interacts with DNA

(A) Composite qRT-PCR analysis of *Ifnb* expression in WT and *Nlrc3*$^{-/-}$ MEFs after HSV-1 infection for 6 and 9 h from three experiments.

(B) Streptavidin pull-down assays of the binding of biotin-HSV-60 dsDNA to indicated HA-tagged proteins in HEK293T cells.

(C) Similar to (B) except HA-NLRC3 was tested and unlabelled HSV-60 dsDNA or LPS was added as a competitor.

(D) PCR analysis of HSV-60 dsDNA bound to NLRC3 or NLRX1 in HEK293T cells. Data are representative of three independent experiments.

(E) Streptavidin pull-down assays of the binding of biotin-HSV-60 (up) or -HSV-15 (down) dsDNA to cell-free, recombinant NLRC3^{FL} or NLRX1^{FL}.

(F) Electrophoretic mobility shift assay (EMSA) of HSV-60 dsDNA binding with cell-free, recombinant NLRC3^{FL}, cGAS^{FL}, or NLRX1^{FL}. Red star represents complex of protein and HSV-60; green star represents free HSV-60.

All experiments were repeated at minimum of three times. Error bars show SEM. Significance was determined by a two-tailed Student's t test (A) or one-way ANOVA (D): **p < 0.01; ****p < 0.0001; and NS, not significant. Please also see Figure S1.

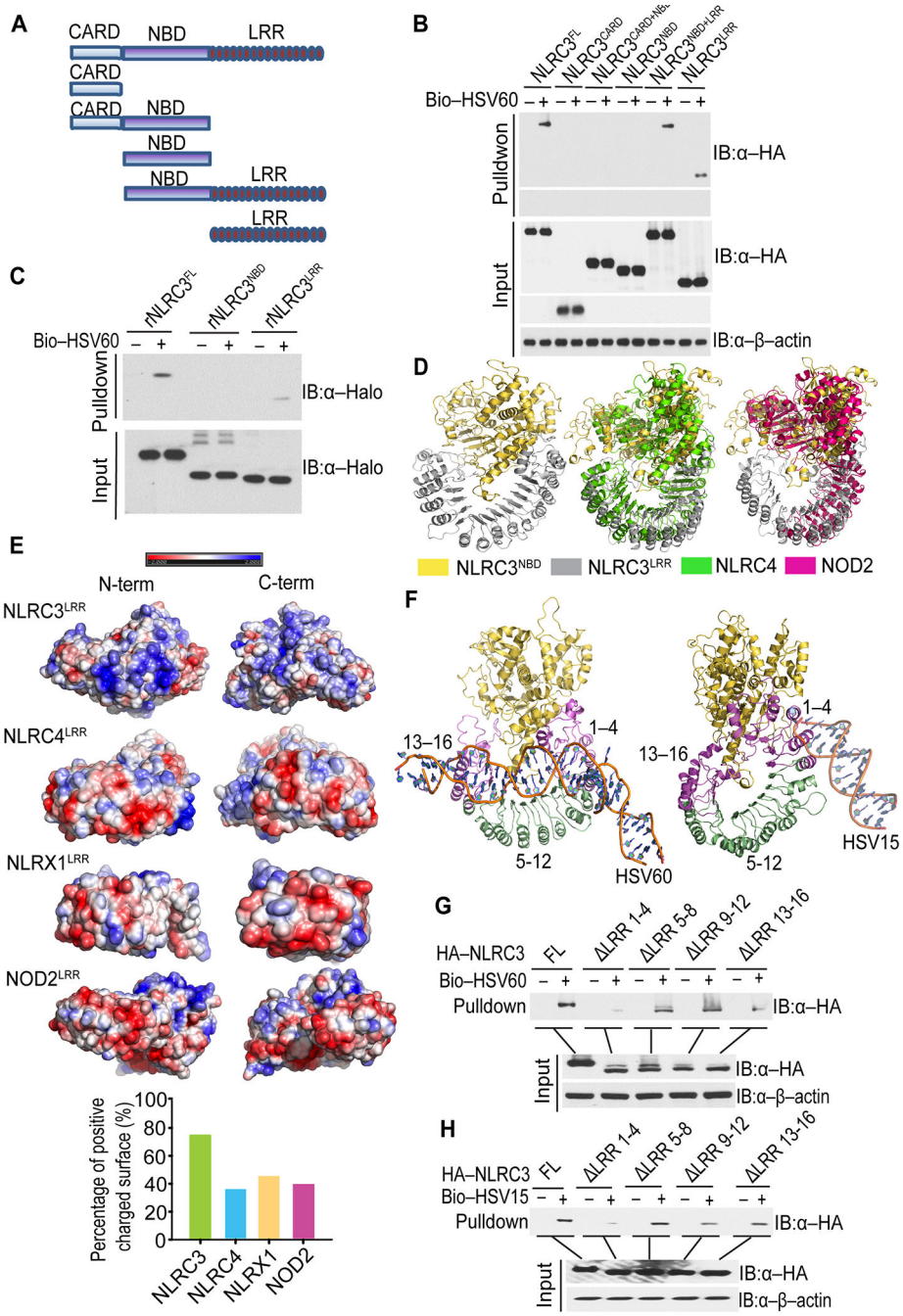

Figure 2. NLRC3 LRR Domain Binds dsDNA

(A) Schematic diagram of NLRC3 domains and deletion mutants.

(B) Streptavidin pull-down assay for the binding of biotin-HSV-60 dsDNA to HA-tagged full-length or indicated domains of NLRC3 in HEK293T cells.

(C) Streptavidin pull-down assay of the binding of biotin-HSV-60 dsDNA to cell-free, recombinant $NLRC3^{FL}$, $NLRC3^{NBD}$, or $NLRC3^{LRR}$.

(D) Homology structural model of NLRC3. Alignment of $NLRC3^{NBD}$ (yellow), $NLRC3^{LRR}$ (gray), NLRC4 (green), and NOD2 (pink) is shown.

(E) Electrostatic potential surface maps of the N and C termini of $NLRC3^{LRR}$, $NLRC4^{LRR}$, $NLRX1^{LRR}$, and $NOD2^{LRR}$.
(F) Computationally derived binding model of $NLRC3^{NBD\text{-}LRR}$ with HSV-60 (left) and HSV-15 (right) dsDNA. NLRC3, LRR1-4, and LRR13-16 are highlighted in purple.
(G and H) Streptavidin pull-down assay of HANLRC3 LRR domain mutants in HEK293T cells.The input lysates were divided into equal halves for subsequent streptavidin pull-down with or without biotin-HSV-60 (G) or HSV-15 dsDNA (H).
All data shown are representative of at least three independent experiments. Please also see Figure S2.

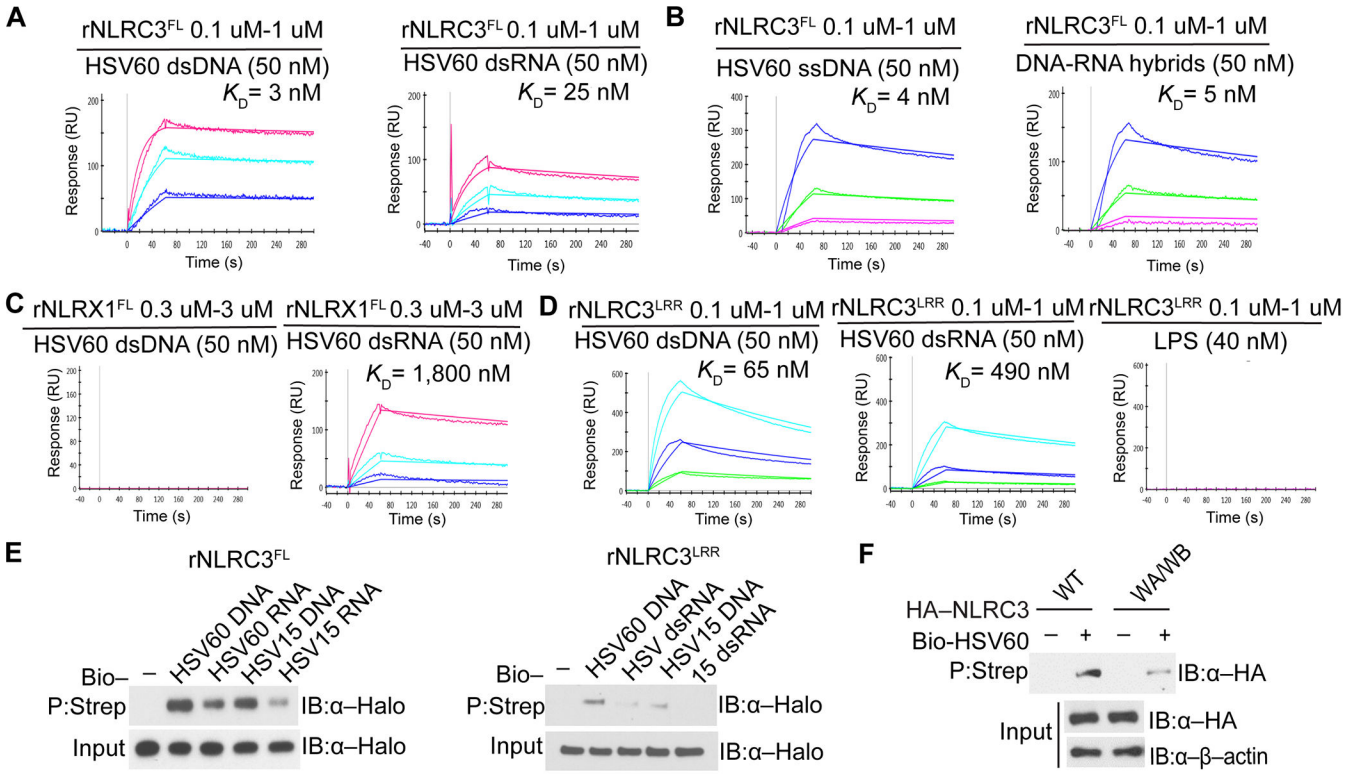

Figure 3. Surface Plasmon Resonance Measurements of Binding Affinities of NLRC3 and Nucleic Acids

(A) Sensorgrams (response unit [RU] versus time) of recombinant NLRC3^{FL} binding to chip-immobilized biotin-HSV-60 dsDNA or dsRNA after subtraction of the control signal. Colored lines indicate different analyte concentrations. Calculated equilibrium dissociation constants (K_D) are indicated.

(B) Sensorgrams of recombinant NLRC3^{FL} binding to chip-immobilized biotin-HSV-60 ssDNA or DNA-RNA hybrids.

(C) Sensorgrams of recombinant NLRX1^{FL} binding to chip-immobilized biotin-HSV-60 dsDNA or dsRNA.

(D) Sensorgrams of recombinant NLRC3^{LRR} binding to chip-immobilized biotin-HSV-60 dsDNA or dsRNA or biotin-LPS.

(E) Streptavidin pull-down assay of the binding of biotinylated nucleic acids to recombinant NLRC3^{FL} or NLRC3^{LRR}.

(F) Streptavidin pull-down assay of the binding of biotin-HSV-60 dsDNA to HA-tagged WT and Walker A/B mutant of NLRC3 in HEK293T cells.

All data shown are representative of three independent experiments. Please also see Figure S2.

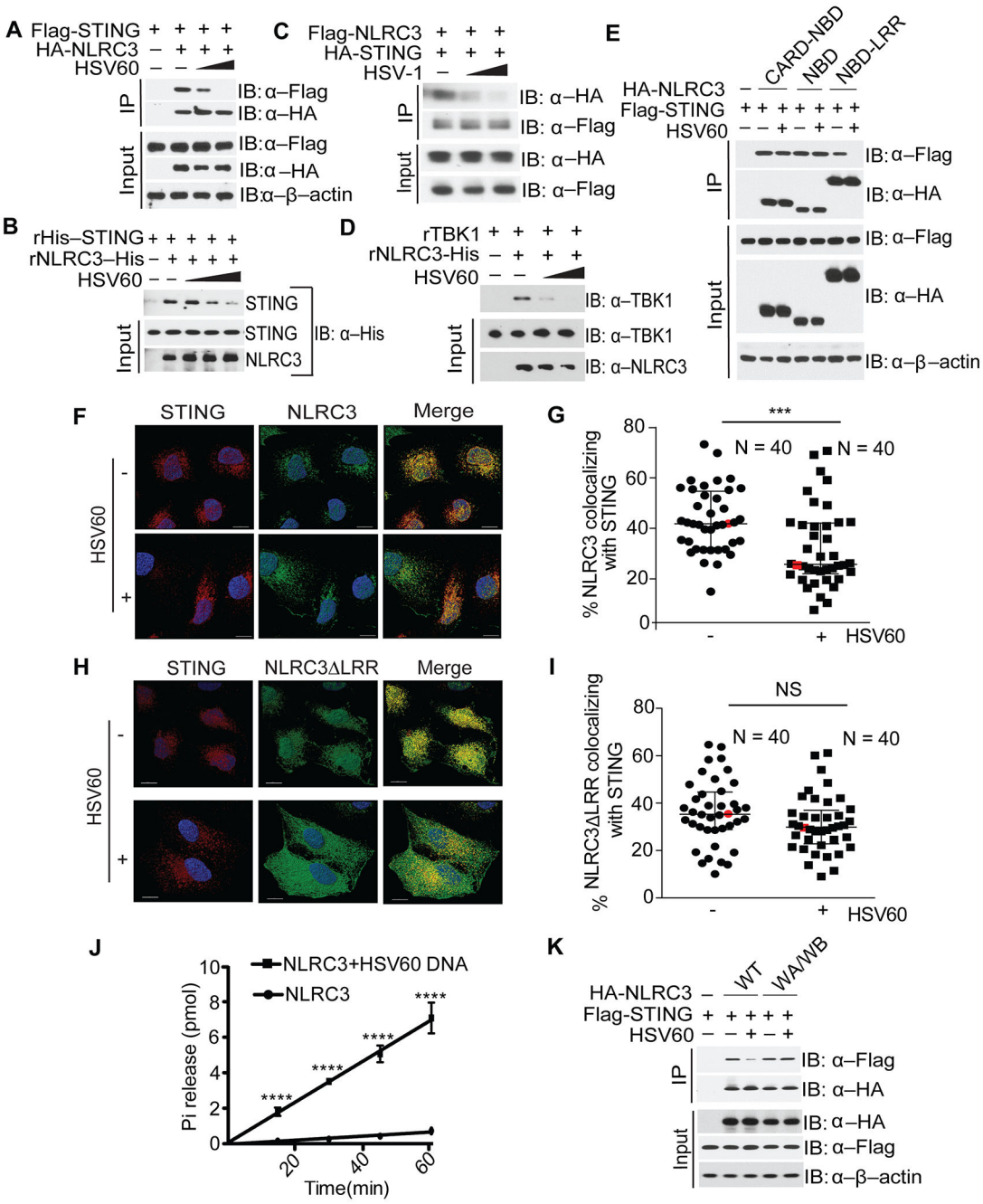

Figure 4. DNA Reduces NLRC3 and STING Interaction

(A) α-HA immunoprecipitates from HEK293T cells transfected with indicated constructs and increasing HSV-60 dsDNA.

(B) Halo-resin pull-down of recombinant NLRC3^{FL} and co-precipitated recombinant STING$^{155-341}$ with HSV60 dsDNA.

(C) α-Flag immunoprecipitates of HA-STING with Flag-NLRC3 is reduced upon HSV-1 infection.

(D) Halo-resin pull-down of recombinant $NLRC3^{FL}$ and co-precipitated recombinant TBK1 with HSV-60 dsDNA.
(E) α-HA immunoprecipitates of Flag-STING with HA-tagged $NLRC3^{CARD+NBD}$, $NLRC3^{NBD}$, or $NLRC3^{NBD+LRR}$ with or without HSV-60 dsDNA in HEK293T cells.
(F) 3D surfaces showing NLRC3-3Flag (green) co-localization with STING-HA (red) in HeLa cells with or without Cy5-HSV-60 dsDNA. Nuclei were stained with 4′,6-diamidino-2-phenylindole (DAPI).
(G) Quantitation of 40 fields from the same sample as (F) with median and interquartile range (n = 40 per group). Red data points represent images in (F). Each dot represents one cell.
(H) 3D surfaces showing NLRC3ΔLRR (green) co-localization with STING(red) in HeLa cells expressing NLRC3ΔLRR-3×Flag and STING-HA ± Cy5-HSV-60 dsDNA. Nuclei were stained with DAPI.
(I) Quantitation of 40 fields from (H) with median and interquartile range (n = 40/group). Red data points represent images in (H). Each dot represents one cell.
(J) PO_4 release from [γ-^{33}P]ATP with purified re-combinant NLRC3 ± HSV-60 DNA (n = 3/group).
(K) α-HA immunoprecipitates of HA-NLRC3 wild-type (WT) or Walker A/B (WA/WB) mutant with Flag-STING in the presence or absence of HSV-60 dsDNA in HEK293T cells.
All experiments were repeated three times. Representative blots in (A)–(E) and (K) are displayed from at least three independent experiments. Error bars in (G), (I), and (J) show SEM. Significance was determined by a two-tailed Student's t test: ***$p < 0.001$; ****$p < 0.0001$; and NS, not significant. Please also see Figures S2–S4.

KEY RESOURCES TABLE

REAGENT or RESOURCE	SOURCE	IDENTIFIER
Antibodies		
Mouse Anti-NLRC3	Santa Cruz	Cat#sc-398947
Rabbit Anti-HA	Cell Signaling	Cat#3724; RRID: AB_1549585
Rabbit Anti-Flag	Cell Signaling	Cat#14793; RRID: AB_2572291
Mouse Anti-Halo	Promega	Cat#G9211; RRID: AB_2688011
Mouse Anti-His	GenScript	Cat#A00186-100; RRID: AB_914704
Mouse anti-HA	Sigma	Cat#H3663; RRID: AB_262051
Rabbit anti-Flag	Sigma	Cat#F7425; RRID: AB_439687
Goat anti-mouse IgG	Invitrogen	Cat#A-11003; RRID: AB_141370
Goat-anti-rabbit IgG	Invitrogen	Cat#A-11008; RRID: AB_143165
Chemicals		
DMEM	GIBCO	Cat#12430-05
Fetal Bovine Serum	SigmaAldrich	Cat#F7305
β-mercaptoethanol	SigmaAldrich	Cat#M6250
TRIzol	Thermofisher	Cat#1559602
SYBR Green Master Mix	Thermofisher	Cat#4344463
NP-40 lysis buffer	Boston BioProducts	Cat#BP-119
EDTA-free Protease inhibitor	Roche	Cat#11873580001
Streptavidin Sepharose beads	Sigma	Cat#GE17-5113-01
Mouse Anti-HA agarose beads	Sigma	Cat#E6779
Polybrene	Sigma	Cat#H9268
Puromycin	Sigma	Cat#P8833
G418	Thermofisher	Cat#10131035
Doxycycline hyclate	Sigma	Cat#D9891
Lipofectamine2000	Thermofisher	Cat#11668019
Aqua Polymount	Polysciences	Cat#18606-20
6% Novex DNA Retardation gel	Invitrogen	Cat#EC6365BOX
Nylon membrane	Schleicher & Schuell	Cat#32-10416216
CHAPS	Thermo Fisher	Cat#28299
Streptavidin Magnetic Particles	Roche	Cat#11641778001
ProteOn NLC sensor chip	Bio-Rad	Cat#1765021
SureBeads Protein G Magnetic beads	Bio-Rad	Cat#161-4021
Proteinase K-Ambion	Thermo Fisher	Cat#AM2546
Mouse IL-1 beta Antibody	R&D systems	Cat#AF-401-NA
Critical Commercial Assays		
Phusion Site-Directed Mutagenesis Kit	Thermofisher	Cat#F541
Lighshift Chemiluminescent EMSA kit	Therofisher	Cat#20148

REAGENT or RESOURCE	SOURCE	IDENTIFIER
Antibodies		
Mouse IL-1β ELISA MAX Standard	BioLegend	Cat#432601
Recombinant DNA		
pcDNA3.1-HA-NLRC3	This paper	N/A
pcDNA3.1-HA-NLRX1	This paper	N/A
pcDNA3.1-HA-STING	This paper	N/A
pcDNA3.1-Flag-NLRC3	This paper	N/A
pcDNA3.1-Flag-STING	This paper	N/A
pcDNA3.1-Flag-RIG-I	This paper	N/A
pcDNA3.1-HA-NLRC3ΔLRR1-4	This paper	N/A
pcDNA3.1-HA-NLRC3ΔLRR5-8	This paper	N/A
pcDNA3.1-HA-NLRC3ΔLRR9-12	This paper	N/A
pCDNA3.1-HA-NLRC3ΔLRR13-16	This paper	N/A
pCIG2-PURO-hNLRC3-3×Flag	This paper	N/A
pCIG2-IRES-PURO	Petrucelli et al., 2012	N/A
pIndcer20-NLRC3-3×Flag	This paper	N/A
pUNO1-hcGAS-Flag	Provided by Dr. Blossom Damania	N/A
pCW-hSTING-HA	Provided by Dr. Stanley Lemon	N/A
pET-28(a)-mouse cGAS	This paper	N/A
pET-28(a)-human STING255-341	Provided by Dr. Pingwei Li	N/A
pDB-His-MBP-hman ASC1-106	Provided by Dr. Joseph A. Duncan	N/A
pcDNA3.1-HA-DDX41	Provided by Dr. Yongjun Liu	N/A
pcDNA3.1-HA-IFI16	Provided by Dr. Yongjun Liu	N/A
Experimental Models: Cell Lines		
HEK293T	ATCC	N/A
HeLa	ATCC	N/A
Experimental Models: Organisms/Strains		
Mouse: C57BL/6J	Jackson Lab	Cat#000664
Mouse: B6.*Nlrc3*$^{-/-}$	Ting Lab	Schneider et al., 2012b
Oligonucleotides		
Please see Table S2	Integrated DNA Technologies	N/A
Software and Algorithms		
GraphPad Prism 6.0	GraphPad Software	https://www.graphpad.com
IMARIS	IMARIS software	http://www.bitplane.com/
ProteOn Manager Software	Bio-Rad ProteON XPR36	http://www.bio-rad.com/
Gromacs	Gromacs 4.6.3	http://www.gromacs.org/
I-TASSER	I-TASSER	https://zhanglab.ccmb.med.umich.edu/I-TASSER/
Haddock web server	HADDOCK2.2	https://haddock.science.uu.nl/